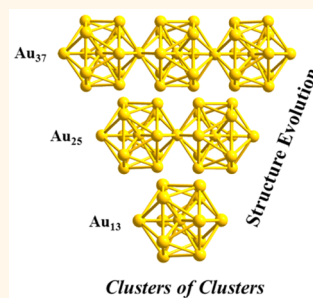


Tri-icosahedral Gold Nanocluster [Au₃₇(PPh₃)₁₀(SC₂H₄Ph)₁₀X₂]⁺: Linear Assembly of Icosahedral Building Blocks

Renxi Jin,^{†,‡} Chong Liu,[§] Shuo Zhao,[†] Anindita Das,[†] Hongzhu Xing,[‡] Chakicherla Gayathri,[†] Yan Xing,^{*,‡} Nathaniel L. Rosi,[§] Roberto R. Gil,[†] and Rongchao Jin^{*,†}

[†]Department of Chemistry, Carnegie Mellon University, Pittsburgh, Pennsylvania 15213, United States, [‡]School of Chemistry, Northeast Normal University, Changchun, Jilin 130024, China, and [§]Department of Chemistry, University of Pittsburgh, Pittsburgh, Pennsylvania 15213, United States

ABSTRACT The [Au₃₇(PPh₃)₁₀(SR)₁₀X₂]⁺ nanocluster (where SR = thiolate and X = Cl/Br) was theoretically predicted in 2007, but since then, there has been no experimental success in the synthesis and structure determination. Herein, we report a kinetically controlled, selective synthesis of [Au₃₇(PPh₃)₁₀(SC₂H₄Ph)₁₀X₂]⁺ (counterion: Cl⁻ or Br⁻) with its crystal structure characterized by X-ray crystallography. This nanocluster shows a rod-like structure assembled from three icosahedral Au₁₃ units in a linear fashion, consistent with the earlier prediction. The optical absorption and the electrochemical and catalytic properties are investigated. The successful synthesis of this new nanocluster allows us to gain insight into the size, structure, and property evolution of gold nanoclusters that are based upon the assembly of icosahedral units (*i.e.*, cluster of clusters). Some interesting trends are identified in the evolution from the monoicosahedral [Au₁₃(PPh₃)₁₀X₂]³⁺ to the bi-icosahedral [Au₂₅(PPh₃)₁₀(SC₂H₄Ph)₅X₂]²⁺ and to the tri-icosahedral [Au₃₇(PPh₃)₁₀(SC₂H₄Ph)₁₀X₂]⁺ nanocluster, which also points to the possibility of achieving even longer rod nanoclusters based upon assembly of icosahedral building blocks.



KEYWORDS: Au₃₇ nanocluster · mixed ligands · clusters of clusters · structure evolution · CO oxidation

Gold nanoparticles have long been a subject of intensive research in the field of nanoscience owing to their important plasmon resonance properties and extraordinary stability.^{1,2} When the size of nanoparticles reaches the ultrasmall size regime (*e.g.*, less than 2 nm), such ultrasmall nanoparticles become nonplasmonic and are classified as nanoclusters. In recent research, atomically precise nanoclusters of molecular purity have been realized,³ and they can be represented by definite molecular formulas (Au_{*n*}L_{*m*}, where *n* represents the precise number of gold atoms and *m* the number of ligands). These nanoclusters exhibit unique geometric structures and molecular-like single-electron transitions dictated by the quantum size effect.^{4–6} Beside the thiolate-protected gold nanoclusters,^{7–12} there has been a renewed interest in phosphine-protected nanoclusters^{13–27} since the earlier works.^{28–33} Theoretical work on gold–phosphine nanoclusters has also been carried out.^{34–39} Among the structural building blocks, the icosahedral motif has been frequently observed in

nanoclusters protected by phosphine, thiolate, or mixed ligands. Of particular interest is how the larger nanoclusters are built up with the smaller building blocks such as Au₁₁ and Au₁₃.^{15,16,31} Several growth modes have been identified, such as vertex-, edge-, or face-sharing. In particular, Teo *et al.* identified a quite common growth mode termed *cluster of clusters via vertex-sharing*,³³ which is reminiscent of atom packing into clusters such as the linear M₂, triangular M₃, tetrahedral M₄, and so on, but here M also represents icosahedral 13-atom building blocks. For such multiunit superstructures, it is of interest to find out whether the properties of the building blocks are preserved and any new collective characteristics would originate from the assembled superstructure.

In recent years, new progress has been achieved in the synthesis and structural characterization of gold cluster of clusters. Bi-icosahedral [Au₂₅(PPh₃)₁₀(SR)₅Cl₂]²⁺ nanoclusters have been successfully synthesized by “bottom-up” or “size-focusing” methods.^{40–42} Single-crystal X-ray crystallography

* Address correspondence to xingy202@nenu.edu.cn, rongchao@andrew.cmu.edu.

Received for review June 10, 2015 and accepted July 20, 2015.

Published online July 27, 2015 10.1021/acs.nano.5b03524

© 2015 American Chemical Society

revealed that the Au₂₅ core was constructed by two icosahedral Au₁₃ units by sharing one vertex gold atom.^{40,41} Compared to the optical absorption spectrum of the icosahedral Au₁₃ cluster,^{14,40} the Au₂₅ nanocluster shows a new electronic transition at long wavelength due to the dimeric structure,⁴³ while other electronic properties are almost preserved compared to the individual icosahedral Au₁₃ nanocluster. From then on, researchers started to study the evolution of structure-related properties by linear assembly of icosahedral Au₁₃ building blocks into longer gold clusters of clusters.^{43,44} Nobusada *et al.* theoretically predicted the structure and electronic properties of a linear tri-icosahedral gold cluster ([Au₃₇(PPh₃)₁₀(SCH₃)₁₀Cl₂)⁺) in 2007.⁴³ However, there has been no experimental success in the synthesis of the tri-icosahedral Au₃₇ nanocluster due to the increasing difficulty in linearly assembling more icosahedral Au₁₃ units together, albeit a cyclic 37-atom tri-icosahedral Ag–Au structure was reported in much earlier work.³³ Generally, it remains a challenge to obtain higher-order Au nanoclusters by using ultrasmall Au clusters as the building blocks.

In this work, we report the successful synthesis of the [Au₃₇(PPh₃)₁₀(SC₂H₄Ph)₁₀Cl₂)⁺ nanocluster after its prediction by Nobusada *et al.* 8 years ago. The Au₃₇ core comprises three icosahedral Au₁₃ building blocks linearly assembled together *via* vertex-sharing, consistent with the theoretical prediction.⁴³ Compared to the previously reported [Au₂₅(PPh₃)₁₀(SC₂H₄Ph)₅Cl₂)²⁺ and [Au₁₃(PPh₃)₁₀X₂)³⁺ nanoclusters, distinct features in the electronic transitions and optical spectra are identified. We have also investigated the catalytic activity of [Au₃₇(PPh₃)₁₀(SC₂H₄Ph)₁₀Cl₂)⁺ as well as the effect of ligands on carbon monoxide (CO) oxidation using anatase TiO₂ as the support for the nanoclusters. The [Au₃₇(PPh₃)₁₀(SC₂H₄Ph)₁₀Cl₂)⁺ nanocluster is so far the largest linear structure in the family of gold “clusters of clusters” and indicates the possibility of further elongation to obtain even longer rod structures.

RESULTS AND DISCUSSION

Synthesis and Characterization of [Au₃₇(PPh₃)₁₀(SC₂H₄Ph)₁₀X₂)⁺. The synthesis of Au₃₇ includes two primary steps: (1) synthesis of the phosphine-capped Au clusters (size mixed) and (2) addition of thiol to convert the phosphine-protected polydisperse Au clusters into phosphine/thiolate-protected monodisperse clusters. It is worth commenting on the critical difference between the syntheses of Au₃₇ and Au₂₅ nanoclusters. The two stages for synthesizing Au₃₇ and Au₂₅ are indeed similar,⁴¹ except that ice-cold water is used as the solvent to dissolve NaBH₄ for reducing the Au(I)–PPh₃ intermediate in the current synthesis of Au₃₇, as opposed to EtOH as the solvent to dissolve NaBH₄ for reducing Au(I)–PPh₃ in the previous Au₂₅ synthesis. We found that the solvent is very critical for the

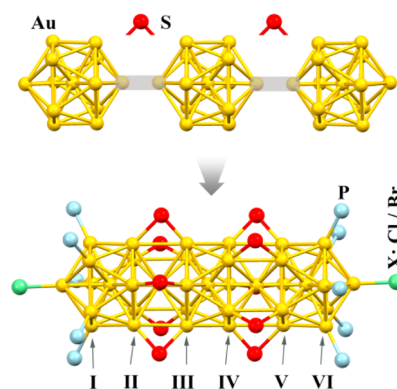
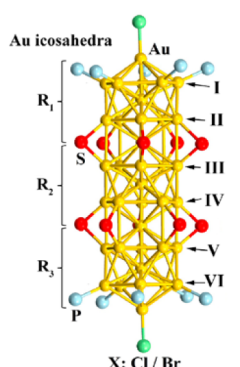


Figure 1. Structure of the [Au₃₇(PPh₃)₁₀(SC₂H₄Ph)₁₀X₂)⁺ nanocluster (color labels: Au, yellow; S, red; P, blue; X: Cl and/or Br, green).

selective synthesis of Au₃₇, which involves kinetic control by tuning the reducing strength of NaBH₄ in different solvents (water vs EtOH) and subsequently the growth kinetics of gold clusters. The success in obtaining the Au₃₇ cluster indicates the future possibility of obtaining even larger clusters based upon linear assembly of smaller building blocks.

The [Au₃₇(PPh₃)₁₀(SC₂H₄Ph)₁₀X₂)⁺ formula and its structure are determined by single-crystal X-ray crystallography. As shown in Figure 1 and Table 1, the Au₃₇ core can be viewed as a linear assembly of three icosahedral Au₁₃ units by sharing vertex gold atoms. There are six pentagonal rings (labeled I–VI in Figure 1). The Au_c–Au_p and Au_p–Au_p bond lengths in each Au₁₃ unit are around 2.76 and 2.9 Å, respectively (where Au_c and Au_p stand for the central and peripheral Au atoms of the Au₁₃ icosahedron, respectively). The icosahedral Au₁₃ units are bridged by thiolate ligands (five thiolates between the II and III layers and another five thiolates between the IV and V layers; Au–S bond length = 2.343 ± 0.068 Å). Ten phosphine ligands are terminally coordinated to the two Au₅ pentagonal rings on the two ends of the rod (*i.e.*, the I and VI layers; Au–P bond length = 2.241 ± 0.041 Å). Two halogen atoms are bonded to two apical Au atoms of the rod (Au–X bond length = 2.479 Å). Of note, the carbon tails of the ligands are not resolved due to disordering. The core structure of [Au₃₇(PPh₃)₁₀(SC₂H₄Ph)₁₀X₂)⁺ is consistent with the earlier theoretical prediction.⁴³ The linear structure of Au₃₇ is in contrast with the other 37-metal-atom tri-icosahedral structures reported previously.^{33,45}

Nuclear magnetic resonance (NMR) is employed to further probe the ligand information on the Au₃₇ nanocluster. ¹H NMR analysis (Supporting Information Figure S1) shows ¹H signals of –CH₂CH₂– of the thiolate ligand at the chemical shifts of 3.15 ppm (integral: 20H), 3.8 ppm (10H), and 4.1 ppm (10H), with a total of 40H (*i.e.*, 10 ligands of –SCH₂CH₂Ph). The aromatic region (6–8 ppm) gives rise to 200H; after the corresponding aromatic 50H of SCH₂CH₂Ph is subtracted, the remaining 150H correspond to 10 ligands

TABLE 1. Bond Lengths of the $[\text{Au}_{37}(\text{PPh}_3)_{10}(\text{SC}_2\text{H}_4\text{Ph})_{10}\text{X}_2]^+$ Nanocluster^a


	Distance Å	
Au-Au	$\text{Au}_c(\text{R}_1)\text{-Au}_p(\text{R}_1)$	2.768 ± 0.029
	$\text{Au}_p(\text{R}_1)\text{-Au}_p(\text{R}_1)$	2.909 ± 0.051
	$\text{Au}_c(\text{R}_1)\text{-Au}_c(\text{R}_2)$	4.897
	$\text{Au}_c(\text{R}_2)\text{-Au}_p(\text{R}_2)$	2.762 ± 0.013
	$\text{Au}_p(\text{R}_2)\text{-Au}_p(\text{R}_2)$	2.904 ± 0.041
	$\text{Au}_c(\text{R}_2)\text{-Au}_c(\text{R}_3)$	5.602
	$\text{Au}_c(\text{R}_3)\text{-Au}_p(\text{R}_3)$	2.768 ± 0.029
	$\text{Au}_p(\text{R}_3)\text{-Au}_p(\text{R}_3)$	2.915 ± 0.053
	$\text{Au}(\text{Layer II})\text{-Au}(\text{Layer III})$	3.059 ± 0.043
	$\text{Au}(\text{Layer IV})\text{-Au}(\text{Layer III})$	3.059 ± 0.043
Au-X:Cl/Br	2.479	
Au-P	2.241 ± 0.041	
Au-S	2.343 ± 0.068	

^a Au_c and Au_p are the central and peripheral Au atoms of the Au_{13} icosahedron, respectively.

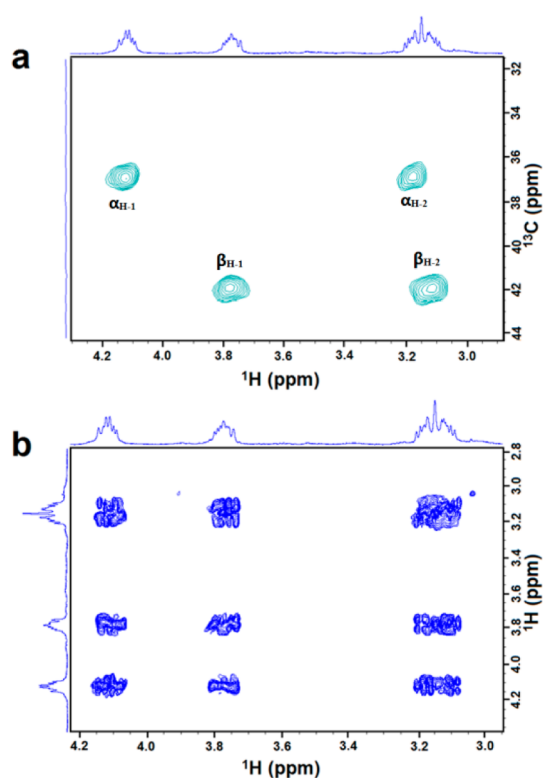


Figure 2. Two-dimensional NMR of the Au_{37} nanocluster: (a) $^1\text{H}\text{-}^{13}\text{C}$ HSQC and (b) $^1\text{H}\text{-}^1\text{H}$ COSY.

of PPh_3 . Thus, the ratio of $\text{PPh}_3/\text{SC}_2\text{H}_4\text{Ph}$ is 1:1, being consistent with the result of the X-ray crystallography. In the HSQC spectrum (Figure 2a), the ^1H signals in the region of 4.2–3.0 ppm show correlations with two different carbons (see the ^{13}C dimension) at 36.8 and 41.8 ppm. Each phenylethylthiolate has α - and β - CH_2 (α and β denote the positions relative to the sulfur atom, with α - CH_2 being closer to the sulfur atom), and thus there would be only one set of $-\text{CH}_2\text{CH}_2-$ in the cluster. However, the $^1\text{H}\text{-}^1\text{H}$ COSY spectrum (Figure 2b) shows that there are four different protons in the region of 4.2–3.0 ppm, which means that each carbon signal

correlates with two different ^1H resonances; that is, the two protons in each methylene (CH_2) group are *not* chemically equivalent. Considering the chemical equivalence of protons in the methylene group in the Au_{25} nanocluster,¹⁶ we conclude that the $-\text{CH}_2\text{CH}_2-$ in Au_{37} is hindered, making one of the protons (labeled $\alpha_{\text{H}-1}$ for α - CH_2 and $\beta_{\text{H}-1}$ for β - CH_2 in Figure 2a) closer to the Au core and the other proton (labeled $\alpha_{\text{H}-2}$ for α - CH_2 and $\beta_{\text{H}-2}$ for β - CH_2 in Figure 2a) farther from the Au core in each methylene group. For the chemical environment of PPh_3 ligands, the ^{31}P NMR spectrum (Figure S2, the chemical shift of the ^{31}P signal is 49.82 ppm) indicates that there is one set of PPh_3 ligands.

The UV–vis–NIR absorption spectrum of $[\text{Au}_{37}(\text{PPh}_3)_{10}(\text{SC}_2\text{H}_4\text{Ph})_{10}\text{X}_2]^+$ exhibits four peaks at 1230, 795, 490, and 430 nm (Figure 3a), which are essentially consistent with the previous prediction based on the density functional theory (DFT).⁴³ The 1230 nm peak arises from the HOMO–LUMO electronic transition, and the 795 nm peak is attributed to the HOMO–1 to LUMO transition. These two peaks are caused by the three interacting Au_{13} icosahedra *via* vertex-sharing. The shorter wavelength peaks at 430 and 490 nm originate in the electronic transitions *within* individual Au_{13} units.⁴³ For the Au_{25} nanocluster (Figure 3b, curve I), the peak at 670 nm is the HOMO–LUMO transition and is caused by the interaction between the two icosahedral Au_{13} units that share one vertex, and the absorption peaks below 500 nm arise from the electronic transitions within individual icosahedral Au_{13} units. For the Au_{13} nanocluster (Figure 3b, curve II), the HOMO–LUMO peak is at 500 nm and the spectral profile is similar to the short wavelength (<500 nm) portions of both Au_{37} and Au_{25} nanoclusters. Taken together, the electronic nature of the individual Au_{13} icosahedron is essentially preserved in the tri-icosahedral Au_{37} nanocluster, but new collective features also emerge; that is, the HOMO–LUMO peak shifts from \sim 500 nm (for the Au_{13} cluster) to 670 nm (for Au_{25}) to 1230 nm (for Au_{37}).

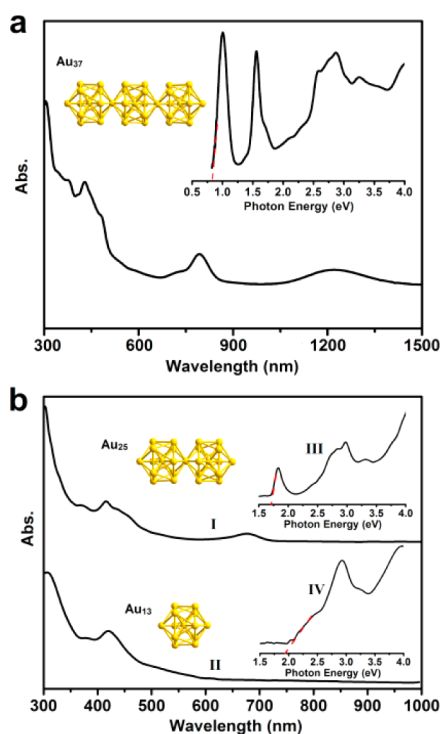


Figure 3. (a) UV-vis-NIR spectra of the Au_{37} nanocluster; inset: spectrum on the photon energy scale. (b) UV-vis spectra of Au_{25} (I) and Au_{13} (II) nanoclusters; inset: spectra of Au_{25} (III) and Au_{13} (IV) on the energy scale.

The optical energy gap of the Au_{37} nanocluster is determined to be 0.83 eV (Figure 3a, inset), which is smaller than that of Au_{25} ($E_g \sim 1.73$ eV, Figure 3b, curve III) and of the Au_{13} cluster ($E_g \sim 1.96$ eV, Figure 3b, curve IV). The observed differences in the optical spectra of Au_{37} , Au_{25} , and Au_{13} illustrate the size evolution of the electronic and optical properties in the clusters of clusters series with increasing numbers of Au_{13} building blocks.

To investigate the electrochemical properties of the Au_{37} nanocluster, we performed cyclic voltammetry (CV) and differential pulse voltammetry (DPV) analyses (Figure S3 and Figure 4). A series of oxidation and reduction peaks are observed in the DPV analysis, corresponding to different oxidation and reduction states of the Au_{37} nanocluster. The first oxidation peak and the first reduction peak are at +0.20 and -0.95 V (vs Ag/AgCl), respectively, thus the electrochemical gap is 1.15 V (the potential difference between the first reduction peak and the first oxidation peak). After the ~ 0.48 V charging energy is subtracted (the difference between the first and second oxidation peaks), the electrochemical gap is converted to the HOMO-LUMO gap of 0.77 eV, which is in agreement with the optical energy gap (0.83 eV). This HOMO-LUMO gap is smaller than that of $[\text{Au}_{25}(\text{PPh}_3)_{10}(\text{SC}_2\text{H}_4\text{Ph})_5\text{Cl}_2]^{2+}$ (1.53 eV) as well as that of $[\text{Au}_{13}(\text{PPh}_3)_8\text{X}_2]^{3+}$ (1.76 eV) but larger than those of the infinite 1D analogues of different charges (the gaps are about 0.3 and 0.2 eV for

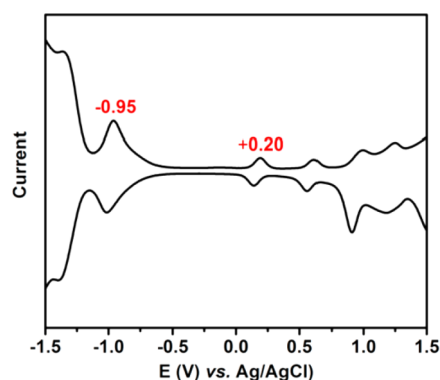


Figure 4. Differential pulse voltammogram of the Au_{37} nanocluster at room temperature.

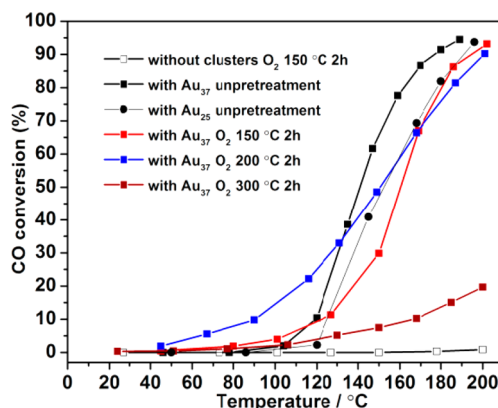


Figure 5. CO oxidation light-off curves of different samples.

the +2 and -2 states of the vertex-sharing wire, respectively), illustrating the general trend—the larger the cluster, the smaller the HOMO-LUMO gap.^{44,46}

Catalytic Activity of $\text{Au}_{37}/\text{TiO}_2$ for CO Oxidation. We further investigated the catalytic activity of the Au_{37} nanocluster toward CO oxidation. Anatase TiO_2 nanorods (Figure S4) were made following a literature approach⁴⁷ and used as the support for the nanoclusters. The $\text{Au}_{37}/\text{TiO}_2$ catalyst was prepared by soaking the TiO_2 powders in a CH_2Cl_2 solution of Au_{37} nanoclusters in a sealed vial for 24 h, followed by drying; no further treatment was done unless otherwise noted. Both the as-prepared TiO_2 rods and the $\text{Au}_{37}/\text{TiO}_2$ catalyst were tested for CO oxidation in a fixed-bed reactor under 1 atm. The light-off curves over the TiO_2 (without clusters) and the $\text{Au}_{37}/\text{TiO}_2$ catalyst are presented in Figure 5. No CO oxidation activity was observed for the bare TiO_2 nanorods below 200 °C (note: moderate activity at higher temperatures). In contrast, the $\text{Au}_{37}/\text{TiO}_2$ catalyst (without any pretreatment) exhibits activity at 100 °C and above, and the $\text{Au}_{25}/\text{TiO}_2$ (without pretreatment) shows activity at 120 °C. For better comparison, we define the T_{50} (the temperature for 50% conversion of CO) and T_{90} (the temperature for 90% conversion of CO) to evaluate the catalysts. As shown in Table S2, the T_{50} and T_{90} temperatures of the $\text{Au}_{37}/\text{TiO}_2$ catalysts are 141 and 176 °C, respectively, which are lower than

those of Au₂₅/TiO₂ ($T_{50} = 152$ °C; $T_{90} = 191$ °C). The Au₃₇/TiO₂ catalyst exhibits turnover frequencies higher than those of Au₂₅/TiO₂ in the entire temperature range (Figure S3), thus Au₃₇ is more catalytically active than Au₂₅. Since Au₃₇ and Au₂₅ have similar structures in terms of atom packing, the enhanced activity of the Au₃₇/TiO₂ catalyst may be attributed to the size effect. Specifically, the Au₃₇ nanocluster contains three icosahedra, and the side facets should constitute the catalytic sites, the number of which are more than that of the Au₂₅ rod.

To study the effect of ligands on CO oxidation, three different pretreatment temperatures (T_{pre} at 150, 200, and 300 °C) were chosen to pretreat the Au₃₇/TiO₂ catalyst in oxygen. Compared with the Au₃₇/TiO₂ catalyst without any pretreatment, the catalytic activity of the pretreated catalysts unexpectedly decreased for the partially ligand-off sample ($T_{\text{pre}} = 150$ or 200 °C). After the ligands were completely removed ($T_{\text{pre}} = 300$ °C), the catalyst showed even lower activity. The decreased activity should be caused by aggregation of the nanoclusters after the ligands were partially or completely removed. It is worth noting that the ligands on the Au₃₇/TiO₂ catalyst showed different behavior when compared with the Au_n/CeO₂ catalysts, in which the catalytic activity would increase after the ligands were partially removed from Au clusters.^{48–50} However, in the current Au₃₇/TiO₂ catalyst, the catalytic activity becomes lower upon ligand removal. The different behavior between these two types of catalysts

may be caused by the different interactions between the Au clusters and the different supports. The bonding force between Au and TiO₂ is weaker than that between Au and CeO₂. After the ligands were removed, the clusters would severely aggregate on the surface of the TiO₂ support, resulting in a decrease in activity, while the CeO₂ support can maintain the cluster structure and the activity was higher due to the formation of more active sites on the cluster surface.

CONCLUSIONS

In summary, we have devised a facile method for synthesizing a new gold *cluster of clusters* ([Au₃₇-(PPh₃)₁₀(SC₂H₄Ph)₁₀X₂]⁺, where X = Cl/Br) protected by mixed phosphine/thiolate ligands. The Au₃₇ core structure with three Au₁₃ icosahedra linearly assembled up is experimentally observed for the first time in gold nanoclusters. The Au₃₇ nanocluster exhibits CO oxidation activity higher than that in the Au₂₅ nanocluster, which illustrates the size dependence in catalysis since their structures are similar (*i.e.*, tricosahedron vs bi-icosahedron). The ligand effect of the cluster on the catalysis has also been investigated. Overall, this new cluster offers valuable information on the size and structure evolution of gold cluster of clusters. Future work may pursue the more elongated rod structures assembled from the icosahedral units. In addition, it is of particular interest whether the linear growth mode of Au₁₃ building blocks can be extended to the case of thiolate-protected nanoclusters.^{51,52}

EXPERIMENTAL METHODS

Synthesis of [Au₃₇(PPh₃)₁₀(SC₂H₄Ph)₁₀Cl₂]⁺. HAuCl₄·3H₂O (0.1 g, dissolved in 3 mL of H₂O) was added into 8 mL of toluene solution of tetraoctylammonium bromide (a phase transfer agent, 0.145 g) with stirring at room temperature for 15 min. After the aqueous phase became clear, which indicated the complete phase transfer of gold salt from aqueous to toluene phase, the aqueous layer was removed. Then, PPh₃ (0.180 g) was added into the above toluene phase under vigorous stirring. The solution became cloudy white immediately. Five milliliters of an aqueous solution of NaBH₄ (0.026 g, dissolved in ice-cold water) was rapidly added to the whitish solution to reduce Au⁺(PPh₃)X (X = Cl or Br) to clusters. After the mixture was stirred for 2 h at room temperature under air environment, toluene was rotavaporated after the removal of the aqueous layer, and the brownish black product was extracted with dichloromethane (DCM). Excess phenylethylthiol (200 μL) was added to this solution and then heated to 313 K. The thermal process was allowed to continue for 36 h at 313 K. The obtained product was washed with methanol and extracted with acetonitrile/DCM = 3:1. The synthetic yield of the [Au₃₇(PPh₃)₁₀(SC₂H₄Ph)₁₀X₂]⁺ was about 5% (Au atom basis). Single crystals were grown by vapor diffusion of diethyl ether into a concentrated solution of the cluster in DCM (5–10 mg in 1 mL of DCM). The synthesis of the [Au₂₅(PPh₃)₁₀(SC₂H₄Ph)₅X₂]²⁺ cluster was carried out under the same experimental parameters except using EtOH as the solvent to dissolve NaBH₄. The thermal process was allowed to continue for 4 h at 313 K, and the obtained product was washed with hexane and extracted with methanol.

Preparation of Au_n/TiO₂ Catalysts. Anatase TiO₂ nanorods were prepared through a hydrothermal process, followed by a simple

annealing.⁴⁷ In a typical procedure, TiO₂ powder (274 mg) and NaOH (19.2 g) were dissolved in H₂O (70 mL) in a beaker. After being vigorously stirred for 1 h, the mixed solution was transferred to a Teflon-lined stainless steel autoclave (15 mL volume) and then sealed to heat at 150 °C. After a 20 h reaction period, the autoclave was cooled to room temperature. The resulting white precipitates were washed with HCl solution (0.1 M), water, and ethanol, and finally dried under vacuum at 60 °C for 4 h. After calcination at 500 °C for 4 h, the anatase TiO₂ nanorods were obtained. For the preparation of supported Au_n/TiO₂ catalysts, 100 mg of the TiO₂ nanorods was impregnated by soaking the powders in a solution of 1 mg of ligated Au_n (Au₂₅ or Au₃₇) nanoclusters in DCM (*ca.* 3 mL) in a sealed vial for 24 h, followed by drying.

Catalytic CO Oxidation. The catalytic oxidation of CO oxidation was conducted under atmospheric pressure in a quartz-tube fixed-bed reactor (8 mm i.d.). One hundred milligrams of the catalyst Au_n/TiO₂ was mixed with quartz sand. A gas mixture of 3% CO/10% O₂/87% He passed through the catalyst bed at a flow rate of 40 mL min⁻¹. The products were analyzed by an online gas chromatograph (HP 6890 series GC) equipped with a TCD detector. The CO conversion was calculated from the measured CO concentration using the formula: CO conversion = [CO_{2-out}/(CO_{out} + CO_{2-out})], where CO_{out} and CO_{2-out} were the outlet CO and CO₂ concentrations, respectively.

Characterization. NMR spectra were obtained on a Bruker Avance 500 spectrometer operating at ambient probe temperature, and ¹H, ¹H–¹³C HSQC, ¹H–¹H COSY, and ³¹P NMR spectra were referenced to probe standards. UV–vis–NIR spectra of gold clusters in DCM were recorded on a Varian Cary 5000 spectrophotometer at room temperature. Differential pulse voltammetry and cyclic voltammograms of the Au₃₇ nanocluster were

measured on a CHI 620C electrochemical station at room temperature. A platinum wire (the counter electrode), platinum working electrode, and Ag/Ag⁺ quasi-reference electrode were used in the electrochemical test. Au₃₇ clusters (~5 mg) were dissolved in ~5 mL of electrolyte solution (0.1 mol/L TBAPF₆ in anhydrous DCM). The solution was bubbled with dry N₂ and blanketed under N₂ throughout the electrochemical measurements. Single X-ray diffraction data of Au₃₇ were collected on a Bruker X8 Prospector Ultra equipped with an Apex II CCD detector and an μ S microfocus Cu K α X-ray source ($\lambda = 1.54178 \text{ \AA}$). Data reduction included absorption corrections with the multiscan method using SADABS (APEX II software suite, Bruker-AXS, 2006). The structures were solved by Patterson methods and refined by full-matrix least-squares using the Bruker program SHELXTL.

Conflict of Interest: The authors declare no competing financial interest.

Supporting Information Available: X-ray crystallographic analysis, 1D NMR spectra of Au₃₇ nanoclusters, and TEM and XRD characterizations of TiO₂. The Supporting Information is available free of charge on the ACS Publications website at DOI: 10.1021/acsnano.5b03524.

Acknowledgment. R.J. acknowledges the scholarship support from the China Scholarship Council. R.J. thanks the Air Force Office of Scientific Research under AFOSR Award No. FA9550-15-1-9999 (FA9550-15-1-0154) for financial support. We thank Dr. Hangjun Ding for UV–vis–NIR measurements.

REFERENCES AND NOTES

- Qian, H.; Zhu, Y.; Jin, R. Atomically Precise Gold Nanocrystal Molecules with Surface Plasmon Resonance. *Proc. Natl. Acad. Sci. U. S. A.* **2012**, *109*, 696–700.
- O'Brien, M. N.; Jones, M. R.; Kohlstedt, K. L.; Schatz, G. C.; Mirkin, C. A. Uniform Circular Disks With Synthetically Tailorable Diameters: Two-Dimensional Nanoparticles for Plasmonics. *Nano Lett.* **2015**, *15*, 1012–1017.
- Jin, R. Atomically Precise Metal Nanoclusters: Stable Sizes and Optical Properties. *Nanoscale* **2015**, *7*, 1549–1565.
- Zhu, M.; Aikens, C. M.; Hollander, F. J.; Schatz, G. C.; Jin, R. Correlating the Crystal Structure of A Thiol-Protected Au₂₅ Cluster and Optical Properties. *J. Am. Chem. Soc.* **2008**, *130*, 5883–5885.
- Guidez, E. B.; Mäkinen, V.; Häkkinen, H.; Aikens, C. M. Effects of Silver Doping on the Geometric and Electronic Structure and Optical Absorption Spectra of the Au_{25-n}Ag_n(SH)₁₈⁻ (n = 1, 2, 4, 6, 8, 10, 12) Bimetallic Nanoclusters. *J. Phys. Chem. C* **2012**, *116*, 20617–20624.
- Schaaff, T. G.; Shafiqullin, M. N.; Khoury, J. T.; Vezmar, I.; Whetten, R. L.; Cullen, W. G.; First, P. N.; Gutiérrez-Wing, C.; Ascensio, J.; Jose-Yacamán, M. J. Isolation of Smaller Nanocrystal Au Molecules: Robust Quantum Effects in Optical Spectra. *J. Phys. Chem. B* **1997**, *101*, 7885–7891.
- Qian, H.; Zhu, M.; Wu, Z.; Jin, R. Quantum Sized Gold Nanoclusters with Atomic Precision. *Acc. Chem. Res.* **2012**, *45*, 1470–1479.
- Luo, Z.; Nachammai, V.; Zhang, B.; Yan, N.; Leong, D. T.; Jiang, D.; Xie, J. Toward Understanding the Growth Mechanism: Tracing All Stable Intermediate Species from Reduction of Au(I)-Thiolate Complexes to Evolution of Au₂₅ Nanoclusters. *J. Am. Chem. Soc.* **2014**, *136*, 10577–10580.
- Mathew, A.; Natarajan, G.; Lehtovaara, L.; Häkkinen, H.; Kumar, R. M.; Subramanian, V.; Jaleel, A.; Pradeep, T. Supramolecular Functionalization and Concomitant Enhancement in Properties of Au₂₅ Clusters. *ACS Nano* **2014**, *8*, 139–152.
- Dainese, T.; Antonello, S.; Gascon, J. A.; Pan, F.; Perera, N. V.; Ruzzi, M.; Venzo, A.; Zoleo, A.; Rissanen, K.; Maran, F. Au₂₅(SET)₁₈, a Nearly Naked Thiolate-Protected Au₂₅ Cluster: Structural Analysis by Single Crystal X-ray Crystallography and Electron Nuclear Double Resonance. *ACS Nano* **2014**, *8*, 3904–3912.
- Zeng, C.; Chen, Y.; Kirschbaum, K.; Appavoo, K.; Sfeir, M. Y.; Jin, R. Structural Patterns at All Scales in A Nonmetallic Chiral Au₁₃₃(SR)₅₂ Nanoparticle. *Sci. Adv.* **2015**, *1*, e1500045.
- Negishi, Y.; Nakazaki, T.; Malola, S.; Takano, S.; Niihori, Y.; Kurashige, W.; Yamazoe, S.; Tsukuda, T.; Häkkinen, H. A Critical Size for Emergence of Nonbulk Electronic and Geometric Structures in Dodecanethiolate-Protected Au Clusters. *J. Am. Chem. Soc.* **2015**, *137*, 1206–1212.
- Shichibu, Y.; Zhang, M.; Kamei, Y.; Konishi, K. [Au₇]³⁺: A Missing Link in the Four-Electron Gold Cluster Family. *J. Am. Chem. Soc.* **2014**, *136*, 12892–12895.
- Shichibu, Y.; Suzuki, K.; Konishi, K. Facile Synthesis and Optical Properties of Magic-Number Au₁₃ Clusters. *Nanoscale* **2012**, *4*, 4125–4129.
- Wan, X. K.; Lin, Z. W.; Wang, Q. M. Au₂₀ Nanocluster Protected by Hemilabile Phosphines. *J. Am. Chem. Soc.* **2012**, *134*, 14750–14752.
- Wang, S.; Meng, X.; Das, A.; Li, T.; Song, Y.; Cao, T.; Zhu, X.; Zhu, M.; Jin, R. A 200-fold Quantum Yield Boost in the Photoluminescence of Silver-Doped Ag_xAu_{25-x} Nanoclusters: The 13th Silver Atom Matters. *Angew. Chem., Int. Ed.* **2014**, *53*, 2376–2380.
- Wan, X. K.; Yuan, S. F.; Lin, Z. W.; Wang, Q. M. A Chiral Gold Nanocluster Au₂₀ Protected by Tetradentate Phosphine Ligands. *Angew. Chem., Int. Ed.* **2014**, *53*, 2923–2926.
- Yang, H.; Wang, Y.; Zheng, N. Stabilizing Subnanometer Ag(0) Nanoclusters by Thiolate and Diphosphine Ligands and Their Crystal Structures. *Nanoscale* **2013**, *5*, 2674–2677.
- McKenzie, L. C.; Zaikova, T. O.; Hutchison, J. E. Structurally Similar Triphenylphosphine-Stabilized Undecagolds, Au₁₁(PPh₃)₂Cl₃ and [Au₁₁(PPh₃)₈Cl₂]Cl, Exhibit Distinct Ligand Exchange Pathways with Glutathione. *J. Am. Chem. Soc.* **2014**, *136*, 13426–13435.
- Chen, J.; Zhang, Q. F.; Bonaccorso, T. A.; Williard, P. G.; Wang, L. S. Controlling Gold Nanoclusters by Diphosphine Ligands. *J. Am. Chem. Soc.* **2014**, *136*, 92–95.
- Das, A.; Li, T.; Nobusada, K.; Zeng, Q.; Rosi, N. L.; Jin, R. Total Structure and Optical Properties of a Phosphine/Thiolate-Protected Au₂₄ Nanocluster. *J. Am. Chem. Soc.* **2012**, *134*, 20286–20289.
- Yanagimoto, Y.; Negishi, Y.; Fujihara, H.; Tsukuda, T. Chiroptical Activity of BINAP-Stabilized Undecagold Clusters. *J. Phys. Chem. B* **2006**, *110*, 11611–11614.
- Zhu, M.; Qian, H.; Meng, X.; Jin, S.; Wu, Z.; Jin, R. Chiral Au₂₅ Nanospheres and Nanorods: Synthesis and Insight into the Origin of Chirality. *Nano Lett.* **2011**, *11*, 3963–3969.
- Kamei, Y.; Shichibu, Y.; Konishi, K. Generation of Small Gold Clusters with Unique Geometries through Cluster-to-Cluster Transformations: Octanuclear Clusters with Edge-sharing Gold Tetrahedron Motifs. *Angew. Chem., Int. Ed.* **2011**, *50*, 7442–7445.
- de Silva, N.; Dahl, L. F. Synthesis and Structural Analysis of the First Nanosized Platinum-Gold Carbonyl/Phosphine Cluster, Pt₁₃[Au₂(PPh₃)₂]₂(CO)₁₀(PPh₃)₄, Containing a Pt-Centered [Ph₃PAu-AuPPh₃]-Capped Icosahedral Pt₁₂ Cage. *Inorg. Chem.* **2005**, *44*, 9604–9606.
- Johnson, G. E.; Priest, T.; Laskin, J. Charge Retention by Gold Clusters on Surfaces Prepared Using Soft Landing of Mass Selected Ions. *ACS Nano* **2012**, *6*, 573–582.
- Pettibone, J. M.; Hudgens, J. W. Synthetic Approach for Tunable, Size-selective Formation of Monodisperse, Diphosphine-protected Gold Nanoclusters. *J. Phys. Chem. Lett.* **2010**, *1*, 2536–2540.
- Briant, C. E.; Theobald, B. R. C.; White, J. W.; Bell, L. K.; Mingos, D. M. P. Synthesis and X-ray Structural Characterization of the Centred Icosahedral Gold Cluster Compound [Au₁₃(PMe₂Ph)₁₀Cl₂](PF₆)₃; the Realization of a Theoretical Prediction. *J. Chem. Soc., Chem. Commun.* **1981**, *5*, 201–202.
- Teo, B. K.; Zhang, H. Polyicosahedrality: Icosahedron to Icosahedron of Icosahedra Growth Pathway for Bimetallic (Au-Ag) and Trimetallic (Au-Ag-M; M = Pt, Pd, Ni) Supraclusters; Synthetic Strategies, Site Preference, and Stereochemical Principles. *Coord. Chem. Rev.* **1995**, *143*, 611–636.

30. Teo, B. K.; Zhang, H. Clusters of Clusters: Self-Organization and Self-Similarity in the Intermediate Stages of Cluster Growth of Au–Ag Supraclusters. *Proc. Natl. Acad. Sci. U. S. A.* **1991**, *88*, 5067–5071.
31. Zhang, H.; Teo, B. K. Stereochemical and Electronic Evidence of Icosahedrality and Polyicosahedrality. *Inorg. Chim. Acta* **1997**, *265*, 213–224.
32. Teo, B. K.; Zhang, H. Cluster of Clusters. Structure of a New 25-Metal-Atom Cluster $[(p\text{-Tol}_3\text{P})_{12}\text{Au}_{13}\text{Ag}_{12}\text{Cl}_7](\text{SbF}_6)_2$ Containing a Nearly Staggered-Eclipsed-Staggered Metal Configuration and Five Doubly Bridging Ligands. *Inorg. Chem.* **1991**, *30*, 3115–3116.
33. Teo, B. K.; Hong, M. C.; Zhang, H.; Huang, D. B. Cluster of Clusters: Structure of the 37-Atom Cluster $[(p\text{-Tol}_3\text{P})_{12}\text{Au}_{18}\text{Ag}_{19}\text{Br}_{11}]^{2+}$ and a Novel Series of Supraclusters Based on Vertex-Sharing Icosahedra. *Angew. Chem., Int. Ed. Engl.* **1987**, *26*, 897–899.
34. Provorse, M. R.; Aikens, C. M. Origin of Intense Chiroptical Effects in Undecagold Subnanometer Particles. *J. Am. Chem. Soc.* **2010**, *132*, 1302–1310.
35. Pei, Y.; Shao, N.; Gao, Y.; Zeng, X. C. Investigating Active Site of Gold Nanoparticle $\text{Au}_{55}(\text{PPh}_3)_{12}\text{Cl}_6$ in Selective Oxidation. *ACS Nano* **2010**, *4*, 2009–2020.
36. Knoppe, S.; Lehtovaara, L.; Häkkinen, H. Electronic Structure and Optical Properties of the Intrinsically Chiral 16-Electron Superatom Complex $[\text{Au}_{20}(\text{PP}_3)_4]^{4+}$. *J. Phys. Chem. A* **2014**, *118*, 4214–4221.
37. Dufour, F.; Fresch, B.; Durupthy, O.; Chaneac, C.; Remacle, F. Ligand and Solvation Effects on the Structural and Electronic Properties of Small Gold Clusters. *J. Phys. Chem. C* **2014**, *118*, 4362–4376.
38. Lugo, G.; Schwanen, V.; Fresch, B.; Remacle, F. Charge Redistribution Effects on the UV–Vis Spectra of Small Ligated Gold Clusters: a Computational Study. *J. Phys. Chem. C* **2015**, *119*, 10969–10980.
39. Muniz-Miranda, F.; Menziani, M. C.; Pedone, A. Assessment of Exchange–Correlation Functionals in Reproducing the Structure and Optical Gap of Organic-Protected Gold Nanoclusters. *J. Phys. Chem. C* **2014**, *118*, 7532–7544.
40. Shichibu, Y.; Negishi, Y.; Watanabe, Ta.; Chaki, N. K.; Kawaguchi, H.; Tsukuda, T. Biicosahedral Gold Clusters $[\text{Au}_{25}(\text{PPh}_3)_{10}(\text{SC}_n\text{H}_{2n+1})_5\text{Cl}_2]^{2+}$ ($n = 2\text{--}18$): A Stepping Stone to Cluster-Assembled Materials. *J. Phys. Chem. C* **2007**, *111*, 7845–7847.
41. Qian, H.; Eckenhoff, W. T.; Bier, M. E.; Pintauer, T.; Jin, R. Crystal Structures of Au_2 Complex and Au_{25} Nanocluster and Mechanistic Insight into the Conversion of Polydisperse Nanoparticles into Monodisperse Au_{25} Nanoclusters. *Inorg. Chem.* **2011**, *50*, 10735–10739.
42. Qian, H.; Zhu, M.; Lanni, E.; Zhu, Y.; Bier, M. E.; Jin, R. Conversion of Polydisperse Au Nanoparticles into Monodisperse Au_{25} Nanorods and Nanospheres. *J. Phys. Chem. C* **2009**, *113*, 17599–17603.
43. Nobusada, K.; Iwasa, T. Oligomeric Gold Clusters with Vertex-Sharing Bi- and Triicosahedral Structures. *J. Phys. Chem. C* **2007**, *111*, 14279–14282.
44. Jiang, D. E.; Nobusada, K.; Luo, W.; Whetten, R. L. Thiolated Gold Nanowires: Metallic versus Semiconducting. *ACS Nano* **2009**, *3*, 2351–2357.
45. Mednikov, E. G.; Dahl, L. F. Nanosized $\text{Pd}_{37}(\text{CO})_{28}\{\text{P}(p\text{-Tolyl})_3\}_{12}$ Containing Geometrically Unprecedented Central 23-atom Interpenetrating Tri-icosahedral Palladium Kernel of Double Icosahedral Units: Its Postulated Metal-core Evolution and Resulting Stereochemical Implications. *J. Am. Chem. Soc.* **2008**, *130*, 14813–14821.
46. Park, S.; Lee, D. Synthesis and Electrochemical and Spectroscopic Characterization of Biicosahedral Au_{25} Clusters. *Langmuir* **2012**, *28*, 7049–7054.
47. Das, K.; Panda, S. K.; Chaudhuri, S. Solvent-Controlled Synthesis of TiO_2 1D Nanostructures: Growth Mechanism and Characterization. *J. Cryst. Growth* **2008**, *310*, 3792–3799.
48. Nie, X.; Zeng, C.; Ma, X.; Qian, H.; Ge, Q.; Xu, H.; Jin, R. CeO_2 -Supported $\text{Au}_{38}(\text{SR})_{24}$ Nanocluster Catalysts for CO Oxidation: A Comparison of Ligand-on and -off Catalysts. *Nanoscale* **2013**, *5*, 5912–5918.
49. Nie, X.; Qian, H.; Ge, Q.; Xu, H.; Jin, R. CO Oxidation Catalyzed by Oxide-Supported $\text{Au}_{25}(\text{SR})_{18}$ Nanoclusters and Identification of Perimeter Sites as Active Centers. *ACS Nano* **2012**, *6*, 6014–6022.
50. Wu, Z.; Jiang, D.; Mann, A. K. P.; Mullins, D. R.; Qiao, Z.; Allard, L. F.; Zeng, C.; Jin, R.; Overbury, S. H. Thiolate Ligands as a Double-Edged Sword for CO Oxidation on CeO_2 Supported $\text{Au}_{25}(\text{SCH}_2\text{CH}_2\text{Ph})_{18}$ Nanoclusters. *J. Am. Chem. Soc.* **2014**, *136*, 6111–6122.
51. Qian, H.; Eckenhoff, W. T.; Zhu, Y.; Pintauer, T.; Jin, R. Total Structure Determination of Thiolate-Protected Au_{38} Nanoparticles. *J. Am. Chem. Soc.* **2010**, *132*, 8280–8281.
52. Malola, S.; Lehtovaara, L.; Häkkinen, H. A DFT Study of Linear Gold–Thiolate Superclusters Absorbing in the Therapeutic NIR Window. *J. Phys. Chem. Lett.* **2014**, *5*, 1329–1334.